Applications of fluorescence lifetime imaging in biology

Manos Protonotarios

Supervisors: Angus Bain & Michael Duchen

CoMPLEX

Essay One,

February 2, 2011

Word Count[1]: 4940

[1] without figures, tables, displayed equations, references, acknowledgments and appendices

Page intentionally left blank

Contents

1 Introduction

Fluorescence Lifetime Imaging Microscopy (FLIM) is a powerful tool in the study of biological processes. One significant opportunity and challenge for FLIM though, is its application on the minimally invasive or non-invasive in situ biopsy, based on natural fluorophores, such as the reduced nicotinamide adenine dinucleotide (NADH) and tryptophan. This has to be combined with data analysis models, whether in time or in frequency domain, that are efficient, reliable and increase the signal-to-noise ratio (especially when the acquisition times are short), such as Global Analysis. Furthermore, mathematical models, such as the Stretched Exponential Function and the Maximum Entropy Method that require less processing load and represent the biophysical mechanisms better than the multiexponential model, particularly when a range of microenvironments is imaged, are necessary in order to provide better tissue differentiation. [1][2][3][4][5][6]

2 Basic Concepts of Fluorescence

2.1 Jablonski Diagram

The basic principles of luminescence (the process of emitting light from molecules with electronically excited states) can be described with the aid of the Jablonski diagram, which illustrates the transitions between the electronic states of a molecule (Appendix A).

2.2 Quantum Yield

The quantum yield Φ, is defined as the ratio of the number of emitted photons n_E from a substance to the number of absorbed photons n_A. Furthermore, if k_r is the emissive rate of the molecule and k_{nr} is the rate of all processes of non-radiative decay then the following equation holds for the quantum yield: [2]

$$\Phi = \frac{n_E}{n_A} = \frac{k_r}{k_r + k_{nr}}$$

2.3 Lifetime

After an infinitely short excitation δ(t) the number of the excited molecules decreases exponentially with time. The fluorescence intensity is proportional to the number of excited molecules and thus it obeys as well the exponential law :

$$I(t) = I_0 \exp\left(-\frac{t}{\tau}\right)$$

In this case the decay is monoexponential and the fluorescence lifetime is the mean time before one molecule fluoresces $\tau = \frac{1}{k_r + k_{nr}}$ or the time when fluorescence intensity drops to the e^{-1} of the initial value I_0. [2][3][7][8]

2.4 Quenching

Many mechanisms can lead to non-radiative transitions to the ground state decreasing the intensity of fluorescence. This phenomenon is called quenching. The quenching when a fluorescent molecule (fluorophore) forms a non-fluorescent complex with another molecule is called static. When the molecules are not chemically altered but the excited state energy is lost by collision of the fluorophore with another molecule, it is called collisional quenching. Many different molecules can act as collisional quenchers such as oxygen and halogens.

The intensity for collisional quenching decreases according to the Stern-Volmer equation:

$$\frac{I_0}{I} = 1 + K[Q] = 1 + k_q \tau_0 [Q]$$

where K is the Stern-Volmer constant, k_q the quenching constant, τ_0 the lifetime without the quencher and [Q] the concentration of the quencher. Excited state chemical reactions and resonance energy transfer can also cause quenching [9][8].

2.5 Forster Resonance Energy Transfer

Forster described quantitatively the resonance energy transfer with quantum mechanics and now it is known as FRET (Forster Resonance Energy Transfer). A fluorophore (donor) is coupled by a dipole-dipole interaction with another molecule (acceptor) so that the excited state energy from the donor is transferred to the acceptor without the emission of light. The rate constant of transfer depends on the fluorescence lifetime of the donor without the acceptor (τ_D) and is very sensitive to the distance between the two molecules, R:

$$k_T(R) = \frac{1}{\tau_D}\left(\frac{R_0}{R}\right)^6$$

R_0 is the critical or Forster radius and depends on the orientation factor $\varkappa^2$, the quantum yield of donor fluorescence without the acceptor Φ_0, the refractive index of the intermediate environment n and the overlap of the emission spectrum of the donor (F_D) and the absorption spectrum (ε_A) of the acceptor which is given by the integral in the following equation:

$$R_0^6 = \frac{9000\ln(10)\kappa^2\Phi_0}{128\pi^5 N_A n^4}\int_0^\infty F_D(\lambda)\ \varepsilon_A(\lambda)\ \lambda^4 d\lambda$$

The orientation factor $\varkappa^2$ depends on the orientation of the transition moments of donor and acceptor. FRET efficiency (i.e. the amount of energy transfer) for a single donor – acceptor pair is given by the equation:

$$E = \frac{R_0^6}{R_0^6 + R^6} = 1 - \frac{\tau_{FRET}}{\tau_D}$$

Meaning that at the Forster distance R_0, E=50%. [2][3][10][11][12]

3 Fluorescence Lifetime Imaging Microscopy

Fluorescence Lifetime Imaging Microscopy (FLIM) is a powerful imaging technique based not on the intensity or the spectrum of fluorescence but on the intensity decay or equivalently the lifetime of the fluorescent molecules. Lifetime, in general, does not depend on light pathway or fluorophore concentration which usually cannot be controlled in biological samples. So, molecules even with the same emitting spectrum and intensity can be differentiated if they have different lifetimes.[2][3][8]

3.1 Time-domain FLIM

The timescale of fluorescence implies that exposure to excitation light very quickly drives the fluorescence to a steady-state of constant illumination as long as the light remains. The intensity or spectrum can then be measured. Steady-state measurements are the result of a statistical average where much information is lost. Time-resolved fluorescence, however, is achieved with a very short (relative to the fluorescence lifetime) light pulse and a rapid detection system to capture the intensity decay. The exciting source can be a pulsed laser or a cheaper LED. Although time-resolved fluorescence requires more advanced equipment, the exact shape of the decay bears important information about the fluorophore and its environment since lifetime is sensitive to refractive index, pH, oxygen, ions etc [8]. [2][3][13] Two categories of instrumentation can be used:

1. Time-Correlated Single Photon Counting (TC-SPC): A scanning repetitive pulsed laser excites the fluorophore pixel-by-pixel and the fluorescence photons are detected by a fast photon multiplier tube (PMT) or a photon avalanche diode. The rate of repetition (MHz) is arranged so as to avoid more than one photons arriving at the detector in one period (Figure 3.2.) but at the same time to ensure that almost all the molecules have relaxed before the next pulse arrives at the pixel. So, the range of lifetimes that can be measured depends on the characteristics of the detector and the repetitive pulsed laser. The implementation can be either confocal or multiphoton. It is a reliable and sensitive (counting individual photons) set up.

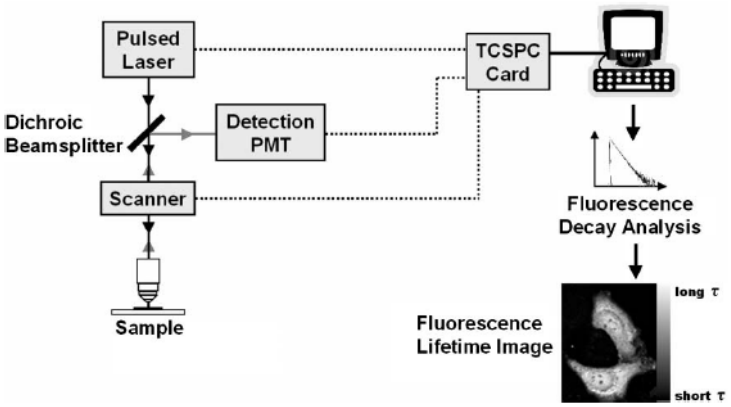

Figure 3.1. Confocal or multiphoton TC-SPC FLIM set up.

(Figure from [3])

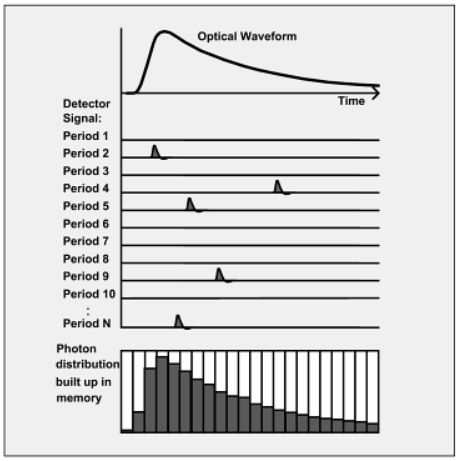

Figure 3.2. TC-SPC principle. Each pixel of the sample is excited by a pulsed laser (pulse duration of picoseconds or femptoseconds) and the time delay between the excitation and the detection of the first photon is recorded. After repeating this procedure many times and representing the number of photons for each delay interval in a histogram, the intensity decay curve is reconstructed. Temporal and spatial resolution is very high. [14][1][13]
(Figure from [14])

2. Wide-field time-gated FLIM: Images recording the intensity of the whole sample are captured with the aid of a high-speed gated camera (charge-coupled device camera - CCD) at specific delays after the excitation pulse and reconstruct the decay curve. All pixels are recorded in parallel, so it is faster than TC-SPC implementation but it lacks accuracy and time resolution.

When very short excitation durations are possible, the limitations of the detector are crucial. The shape of intensity p(t) that the instrument records for an infinitely short fluorescence (instrument response function or IRF of the detector) must be taken into account so as to correct the measurement of the decay data. The observed emission intensity is derived as the convolution of p(t) with the exponentially decaying intensity I(t) that follows a δ(t)-excitation:

$$F(t) = I \otimes p = \sum_{q=1}^{Q} \alpha_q \exp(-\frac{t}{\tau_q}) \otimes p(t)$$

where I(t) is the intensity resulting from the contributions of Q different species with different lifetimes τ_q (different molecules or same molecules in different state) and with each one contributing α_q to the total intensity. A standard method is to use an algorithm of iterative reconvolution to fit the experimental decay curve. In this case a multiexponential [15], [16] fit is necessary, otherwise the calculated lifetime results as an averaged contribution of the decays of all species. [17][18][2]

3.2 Frequency-domain FLIM

Equivalently, in theory, to the short pulse (time-domain FLIM), a sample could be excited by light (laser or LED) modulated in a set of frequencies (frequency-domain FLIM). If a fluorophore is excited by light of a sinusoidally modulated intensity and the frequency ω of modulation is close to the reciprocal of its lifetime, then the intensity of emission is oscillating too at the same frequency but with a phase shift $\Delta\phi_\omega$ and a modulation ratio M_ω.

The following equations, which help to determine the lifetime τ, hold true:

$$\Delta\phi_\omega = \arctan(\omega\tau)$$

$$M_\omega = \frac{1}{\sqrt{1+\omega^2\tau^2}}$$

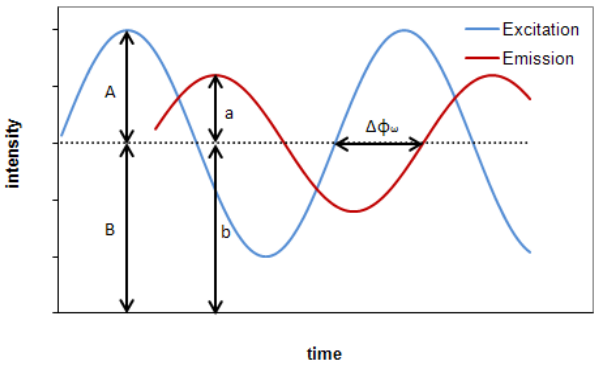

Figure 3.3. Graphical determination of phase shift $\Delta\phi_\omega$ and modulation ratio M_ω in frequency-domain FLIM. $M_\omega = \frac{B/A}{b/a}$ (Figure inspired from [8])

Most interesting cases, however, present complex decay curves as a result of different species in the sample. Then, in order to resolve the different lifetimes τ_q and relative populations a_q of the Q species, measurements of the modulations M_ω and phase shifts $\Delta\phi_\omega$ that correspond to variant frequencies of the modulated excitation field must be recorded. [19][20][21][2][3][8]

The phase shift of each frequency $\Delta\phi_n$ and its modulation M_n are related to the fractional contributions α_q and lifetimes τ_q:

$$\Delta\phi_\omega = \arctan\left(\frac{A_\omega}{B_\omega}\right)$$

$$M_\omega = \sqrt{A_\omega^2 + B_\omega^2}$$

where,

$$A_\omega = \sum_{q=1}^{Q} \frac{\alpha_q \omega\tau_q}{1 + (\omega\tau_q)^2}$$

$$B_n = \sum_{q=1}^{Q} \frac{\alpha_q}{1 + (\omega\tau_q)^2}$$

From phase and modulation data a χ^2 measure is defined, which is a weighted sum of the squared differences between the measured and calculated values ($\Delta\phi_{c\omega}$, $M_{c\omega}$). So, one has to determine the α_q and τ_q for each species by minimizing a χ^2 function, knowing $\Delta\phi_\omega$ and M_ω for each frequency (least-squares problem) (Figure 3.4). [17][19][20][21][22]

$$\chi^2 = \sum_\omega \frac{1}{\sigma^2_{\Delta\phi_\omega}} (\Delta\phi_\omega - \Delta\phi_{c\omega})^2 + \sum_\omega \frac{1}{\sigma^2_{M_\omega}} (M_\omega - M_{c\omega})^2$$

The $\sigma^2_{\Delta\phi_\omega}$ and $\sigma^2_{M_\omega}$ are estimated uncertainties for the measured quantities while reduced χ^2_R is χ^2 divided by the number of degrees of freedom [1].

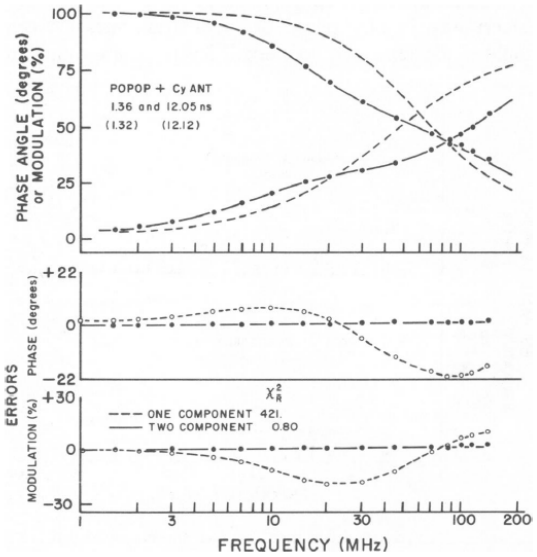

Figure 3.4. Phase shift and modulation data points for a mixture of p-bis[2-(5-phenyloxazolyl)] benze (POPOP) and 9-cyanoanthracene. The dashed line represents the monoexponential fit while the solid one the biexponential fit. It is obvious, from the residuals diagram that the biexponential is a much better fit. (Figure from [19])

In the past, limitations in technology which was necessary for the frequency-domain set up (Acousto-optic modulators (AOMs), image intensifiers, frequency mixing devices etc) impeded frequency-domain FLIM development, but now it is widely used. [8][1]

3.3 FLIM – FRET

Although FRET can be used for the quantification of protein interactions by measuring the intensity of fluorescence, it can be significantly more useful when it is combined with FLIM [2], since FLIM is independent of the spatially varying concentrations of the acceptor and donor, as it is usually the case in biological samples. FRET provides an additional process of depopulation for the excited states resulting in a reduced lifetime [23][24]. Since FRET efficiency is significant only when the distance between the donor and acceptor is extremely small, typically $R<2R_0$, FRET-FLIM microscopy provides an equivalent resolution of the order of 1.5nm to 6nm, which is much higher than the optical resolution limit. [10][8][2][3] With the use of quantitative FRET the actual intramolecular distances, orientations between different parts of a macromolecule and structural and geometrical aspects of single macromolecules can be measured [10].[25][3]

The exact value R_0 for a donor-acceptor pair depends, in general, on the nature of the microenvironment. The orientation factor k^2 is usually taken 2/3 for random and rapidly changing transition moment orientations (isotropic dynamic average) but this is not always correct because of constraints of the microenvironment [1].

3.4 Polarization-Resolved FLIM

Fluorophores absorb photons mostly when the angle of the transition moment with the electric vector is relatively small. When excited with linearly polarized light, the random orientation of the transition dipole results in a selective excitation (photoselection) and consequently in a partially polarized emission along the electric vector of the excitation. The parallel $I_{par}(t)$ and perpendicular $I_{per}(t)$ to the excitation light intensity decays can be measured with a polarizer and give the time-resolved anisotropy function r(t) which is defined as [1]:

$$r(t) = \frac{I_{par}(t) - I_{per}(t)}{I_{par}(t) + 2I_{per}(t)} = \frac{I_{par}(t) - I_{per}(t)}{I(t)}$$

where I(t) is the total intensity. The anisotropy decays monoexponentially (spherical rotor):

$$r(t) = (r_0 - r_\infty)\exp\left(-\frac{t}{\theta}\right) + r_\infty$$

where r_0 is the initial anisotropy, r_∞ is the limiting anisotropy for hindered rotation (otherwise is zero) and θ is the rotational correlation time which is related to the rotational diffusion. In isotropic environment (Debye-Stokes-Einstein)[26]:

$$\theta = \frac{\eta V}{kT}$$

where η is the viscosity of the liquid environment, V the equivalent volume of the molecule, k the Boltzmann constant and T the absolute temperature. Knowledge of θ can provide information on the size and shape of proteins, hindered rotation or viscosity of molecular environments. Moreover, since θ is comparable to most fluorescence lifetimes (order of ns), any variation of θ because of binding or other interaction will be captured by time-resolved FLIM. The Perrin equation can be used to relate steady-state fluorescence anisotropy with the rotational correlation time and the lifetime, when rotations are the main depolarization path:

$$\langle r \rangle = \frac{r_0}{1 + \frac{\tau}{\theta}}$$

Steady-state or time-resolved anisotropy imaging allows the detection of interactions between molecules of identical (homo-FRET) or different (hetero-FRET) proteins, as excitation energy can pass to another molecule with different orientation causing depolarization. Time-resolved intensity and anisotropy measurements with computational modeling have been combined to determine the geometrical arrangement of the 3-Phosphoinositide-dependent kinase1 (PDK1) homodimer molecule[27][28]. [1][3][2][8][7]

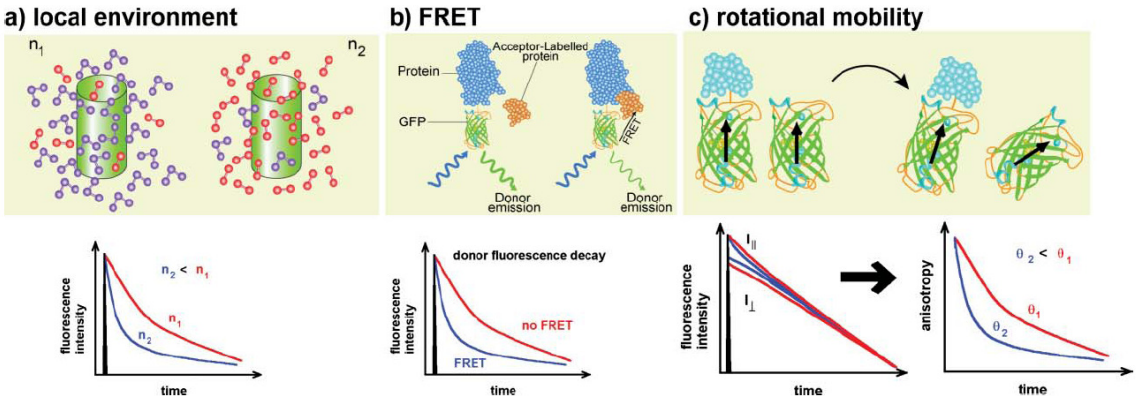

Figure 3.5. Concise presentation of the main FLIM techniques

a) FLIM can be used to probe the cellular environment because lifetime is sensitive to certain environment parameters such as the refractive index (n), pH, oxygen, ions etc.

b) In FLIM-FRET the lifetime of the donor is decreased because of the non-radiative energy transfer to the acceptor. Thus, by the change in the lifetime of the donor, molecular interactions and protein conformational changes can be derived.

c) Anisotropy imaging for the rotational mobility. It can be affected by the viscosity of the solvent and binding or conformational changes.

(Figure from [7])

3.5 Noise in FLIM Microscopy

The detector signal noise depends on the shot noise. Since the number of photoelectrons detected follows the Poisson distribution, the measured signal S gives an estimate of the noise as the SD of the signal:

$$SNR = \frac{S}{\sqrt{S}} = \sqrt{S}$$

It is obvious that as the number of photoelectrons increases, the Signal-to-Noise Ratio (SNR) improves. For example if S=100 is the number of photoelectrons then SNR=10, but if S=10,000 then SNR=100. This is the upper limit for the SNR since the measurement system will add extra noise to the signal, one important component of which is the dark signal noise, meaning photoelectrons that reach the detector in the absence of light. [10][8]

A number of issues are related to the signal and noise values in a FLIM experiment, such as the minimum number of photons to provide a relatively good SNR or a reliable exponential curve, the maximum excitation intensity or exposure time for biological samples before photobleaching, the quantum efficiency of the detector, spectral responses of cameras and PMTs, background noise, efficient data analysis etc. [17][9]

4 FLIM Applications & Techniques

4.1 NADH

4.1.1 The potential of NADH as a cancer probe

Reduced Nicotinamide Adenine Dinucleotide (NADH) is a natural fluorophore and plays fundamental role in the metabolism as an electron carrier in the mitochondria electron transport chain. It has shorter lifetime at free state than when it is bound with enzymes, while this change depends on the enzyme. The fact that cancer cells use aerobic glycolysis instead of oxidative phosphorylation (Warburg effect) and the metabolic pathways change implies that there will be differentiation between the average lifetime of the bound NADH in healthy and cancerous cells. [29][30][31]

4.1.2 Fluorescence Lifetime Imaging Measurement of NADH in the Lab

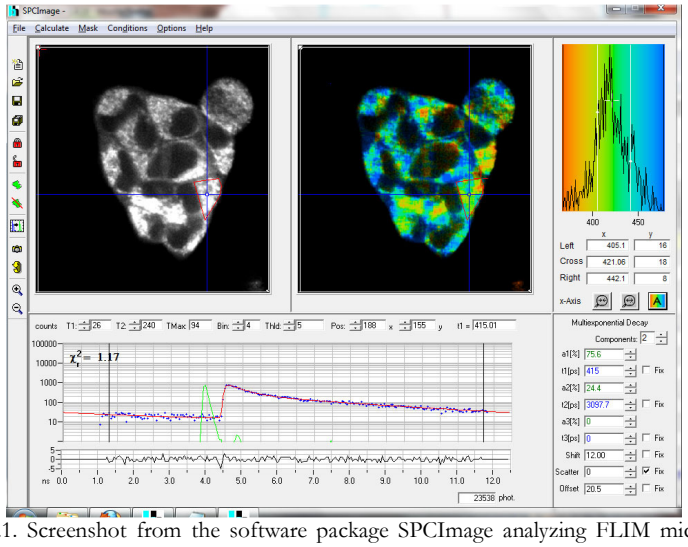

Figure 4.1. Screenshot from the software package SPCImage analyzing FLIM microscopy data. The microscope used was a two-photon Zeiss LSM 510 with Coherent Chameleon laser at 700nm, Becker & Hickl FLIM system.

Top-Left Image: Intensity	Top-Center Image: Lifetime distribution superimposed on intensity	Top-Right Image: Histogram of lifetime distributions for the selected area
Decay for the selected pixel Reduced Chi-square=1.17 Blue points: photon count data Red line: fitted biexponential decay curve Green curve: measured IRF Black curve: weighted residuals Total number of photons (selected pixel): 23538		Biexponential model for the decay α_1=75.6% τ_1=415ps (short component-free) α_2=24.4% τ_2=3097.7ps (long component-bound)
Binning =4 means 9X9 pixel area. Increase in the number of bins means increase in the SNR because more photons are counted but spatial resolution gets worse.		
Measurement of the lifetime of free and bound NADH in cultured HEK (Human Embryonic Kidney) cells was conducted in the Lab of the UCL Research Department of Cell and Developmental Biology, with the guidance and help of PhD student Thomas Blacker. The cells were NADK gene knock-out mutants, so the fluorescence measured originated only from NADH and not NADPH.		

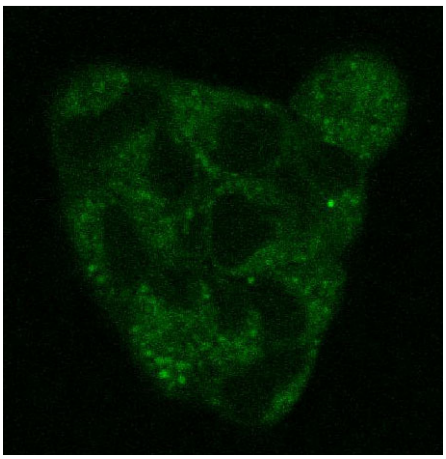

Figure 4.2.a. Fluorescence intensity of the NADH, both free and bound, from an aggregate of HEK cells

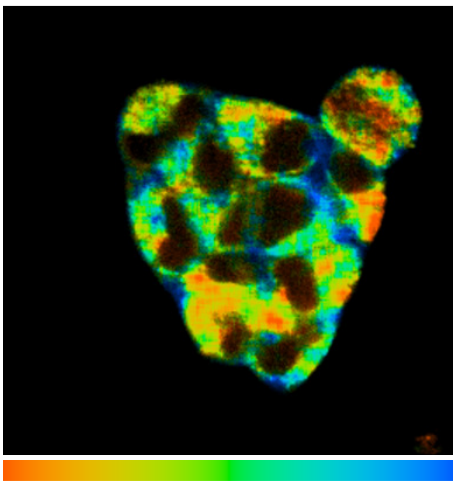

Figure 4.2.b. Distribution of the contribution of bound NADH

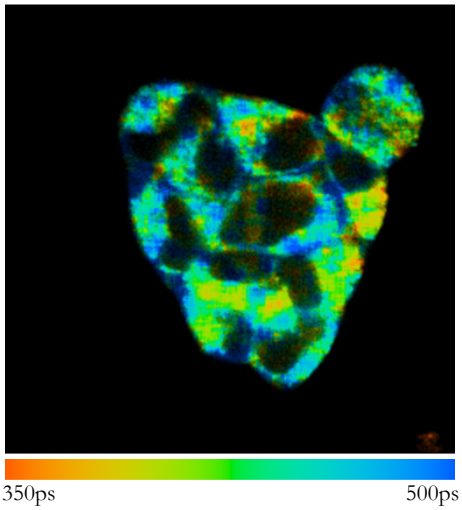

Figure 4.2.c. Distribution of the lifetimes τ_1 (free NADH)

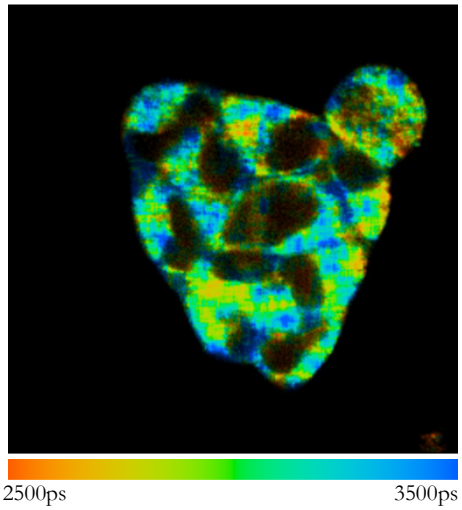

Figure 4.2.d. Distribution of the lifetimes τ_2 (bound NADH)

4.2 Global Analysis

Global analysis is a technique of analyzing data by imposing constraints on them. For example, assuming that some of the parameters are similar or identical in each experiment (global parameters), one can simplify complicated mathematical processing, increase efficiency or/and achieve more reliable results. Global analysis in FLIM, whether in time or frequency domain, mainly assumes that lifetimes of different fluorescent species do not vary spatially, which in most biological applications is true. Thus, in every pixel of an image or in a subset of them, the number of lifetimes is limited to a common set of lifetimes, although the contribution of each species may vary. Global analysis is also used as an approach that equivalently increases SNR for the same excitation times and intensities avoiding longer imaging duration and photobleaching, something crucial for biological samples. Furthermore, the spatial heterogeneity of the samples means that in some pixels the intensity of fluorescence for one or both species - for example, in biexponential decay – can be so low that the fitting is unreliable and the resulting lifetimes have no meaning.[32][33][34][1][3][17]

4.2.1 Application of Global Analysis in time-domain (case 1)

A hybrid method of global analysis and linear algebra is applied by Smirnov and co-workers [35]. A custom-designed program uses global fitting for selected regions of an image. Initiating with guessed values for fractional contributions and lifetimes, it uses a non-linear least squares fitting algorithm to estimate only the lifetimes. Afterwards, linear algebra is used to determine the fractional contributions for each pixel. This method is used with biexponential decay fitting in the case of free and bound NADH revealing uniform concentrations of both, along the isolated cardiac myocyte (Figure 4.3).

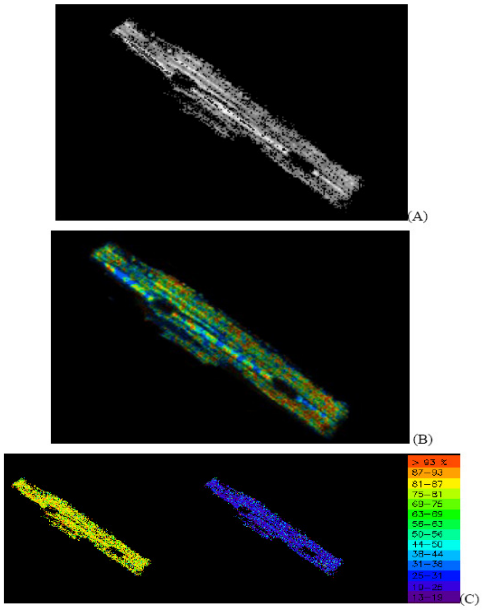

Figure 4.3. Isolated myocyte

(A) Total intensity
(B) Ratio of free to bound NADH with standard software showing punctuate pattern
(C) Amplitudes of free NADH component (left) and bound NADH component (right) showing a relatively uniform concentration

(Figure from [35])

Comment: The authors do not provide a color legend for image B. Such a punctuate image, giving the impression of large difference in concentrations, could result even in the case of relatively constant concentrations if the color code is normalized.

4.2.2 Application of Global Analysis in time-domain (case 2)

With FLIM, the FRET efficiency can be quantified by the change of the donor lifetime when it is in close proximity to the acceptor. Since, however, not only the interacting but also the non-interacting molecules contribute to the average donor lifetime, the measured lifetime is biased towards larger values and the distances calculated are overestimated [11]. Laptenok and co-workers [11], in order to overcome this problem, measure the average rise time of the acceptor intensity immediately after the donor excitation, which as they prove, is the same with the lifetime of the FRET interacting donors (Appendix B). Therefore, by measuring the rise time of the fluorescence of the acceptors, they obtain an accurate estimate of the FRET efficiency. A global analysis in this case makes use of a number of images and assumes that for the multiple datasets the rise and decay times are the same, and compensates for the limiting signal-to-noise ratio. [2] Their approach is presented in Appendix B.

The FRET pairs studied were ECFP(donor)-EYFP(acceptor) (cyan and yellow fluorescent proteins) and EGFP(donor)-m-Cherry(acceptor) (green and red fluorescent proteins) in live plant cells (protoplasts). It is measured that ECFP without FRET presents biexponential decay, so for the FRET it is expected a multiexponential model of at least four lifetimes, which is impossible to give a reliable fit. Therefore, measuring the rise time of the acceptor is a more convenient measurement. The results for the distances of the donor-acceptor pairs were significantly lower than those calculated using the donor lifetime.

4.2.3 Application of Global Analysis in frequency-domain (case 1)

Squire and co-workers [20] present a frequency domain FLIM technique (mfFLIM) in which the sample is excited with light modulated simultaneously by multiple frequencies (Appendix C). This parallel technique is equivalent to the conventional sequential variable frequency though it is faster, has technical advantages and provides better lifetime definition [36][37].

Verveer and co-workers [17] combine the mfFLIM technique with global analysis. For the processing of the excited emission a modulated intensifier (mixer) is used. The time-independent component of the signal at the output of the intensifier is recorded for every pixel and by varying the phase of the intensifier at equal steps a sequence of images is created. With a pixel-by-pixel analysis the time-dependent emission intensity can be reconstructed and so the $\Delta\phi_n$ and M_n for every harmonic can be measured. A non-linear fit can then give the relative populations and lifetimes for each pixel. Alternatively, the "lifetime invariant fit" [37] averages all pixels in an image to increase SNR, estimates afterwards the lifetimes and then calculates the populations from linear equations. Global analysis however [17], leads to a simpler equation for the χ^2, with Q lifetime values and Q-1 (one equation is $\sum_{q=1}^{Q}\alpha_q = 1$) fractional contributions as parameters. Since the minimization of χ^2 becomes a separable nonlinear least squares problem, it can be confronted with already implemented algorithms [38]. The results for simulated data (Figure 4.4) show strong resolving efficiency for the global analysis approach, even with the single frequency modulation.

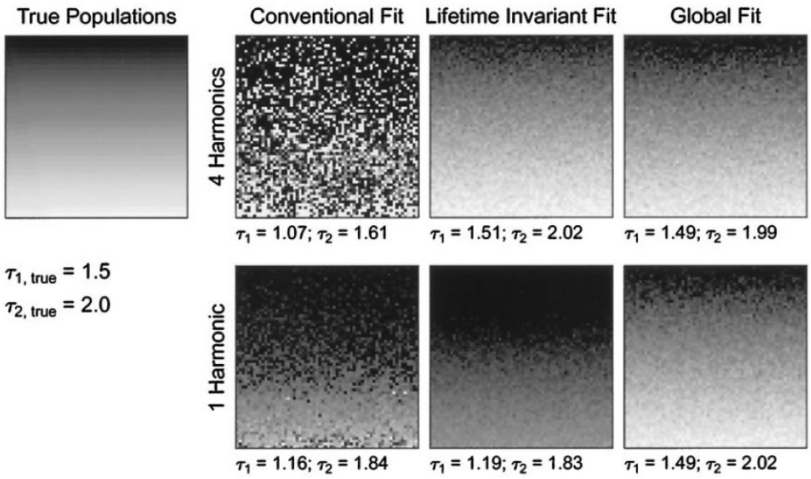

Figure 4.4. The estimated lifetimes for simulated data of biexponential decay curve (1 and 4 harmonics) and relative populations (white or black) for the three approaches. The global analysis approach performs much better. (Figure from [17])

4.2.4 Application of Global Analysis in frequency-domain (case 2)

Wide-field FLIM with global analysis is applied by Verveer and co-workers [39] to quantitatively study FRET for the plasma membrane-bound epidermal growth factor receptor ErbB1 and Cy3 (fluorescent dye) labelled antiphosphotyrosine antibody Cy3/PY72 (acceptor). The ErbB1 is fused to green fluorescent protein EGFP (donor). This technique is used to quantitatively image the biochemical state (phosphorylated or not) for ErbB1 receptors in MCF7 (breast cancer cell line) cells. Conventional analysis is used to ensure that only one lifetime is present for the donor and that any significant change in this will happen because of the FRET. Although lifetimes do not vary spatially, the Point Spread Function (PSF) captures varying populations and the calculations for the lifetimes are affected. Contrary to [20], a deconvolution processing is applied after the global analysis and not before, which proves to be more efficient. Indeed, the resulting FLIM map reveals that after epidermal growth factor (EGF) stimulation the phosphorylated receptors are located only on the membrane and not inside the cytoplasm (Figure 4.5). Moreover their population value is near 100%, meaning that all receptors have reacted. An additional advantage of this method is that correction for photobleaching can be applied before the deconvolution.

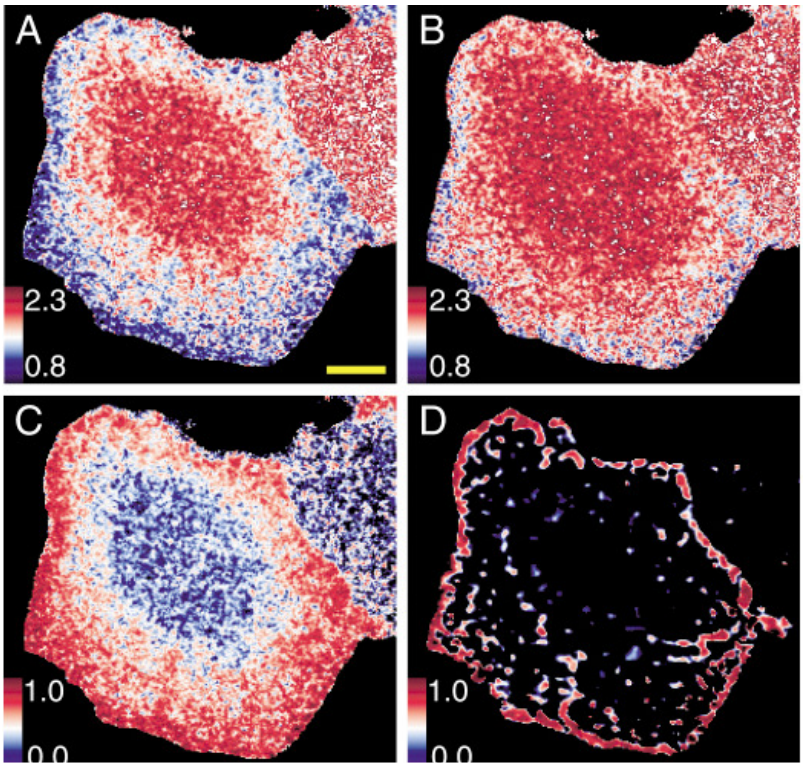

Figure 4.5. A section of MCF7 cell imaged with Frequency-domain FRET-FLIM.

(A) Conventional calculation of the lifetime from phase shifts (ns)

(B) Conventional calculation of the lifetime from modulations (ns)

(C) Populations of phosphorylated ErbB1 receptor calculated with global analysis

(D) Populations of phosphorylated ErbB1 receptor calculated after deconvolution

(Figure from [39])

4.2.5 Application of Global Analysis in frequency-domain (case 3)

Verveer and co-workers [23] determine with global analysis the lifetimes and the relative contributions at each pixel for the ErbB1-GFP, Cy3/PY72 FRET pair of the previous paragraph. They use a single frequency modulation and optimize their algorithm [17] for this simple case. The biexponential decay is fitted successfully with a single modulation frequency, something which is impossible with the pixel-by-pixel analysis. In fact, this advancement is very important because FRET-FLIM with biexponential decay is common while single-frequency instrumentation is cheap and widely used [17].

4.3 Stretched Exponential Function (StrEF)

When the monoexponential model in time-domain FLIM does not accomplish an acceptable fit, more terms are added in order to minimize χ^2 but disanalogous computational demands arise. Moreover, a multiexponential fit, which should also be in accordance with a physical model, has a number of distinct exponentials that in some cases, even though give a good χ^2, seem arbitrary or without physical meaning [15]. For some molecules, furthermore, fluorescence is expected to arise from a continuous distribution of lifetimes, as for example from a single-tryptophan protein which has a large number of different conformations [40][41]. The Kohlrausch-Williams-Watts or StrEF, which describes fluorescence with continuous distribution of lifetimes, is proposed as an alternative approach [35]:

$$I(t) = I_0 \exp\left[-\left(\frac{t}{\tau_{kww}}\right)^{1/h}\right] + const.$$

where τ_{kww} is the decay constant and h the heterogeneity parameter

StrEF can be expressed as a superposition of exponential terms with a continuous distribution of lifetimes $\varrho(\tau)$:

$$I(t) = \int_0^\infty \exp\left(-\frac{t}{\tau}\right)\rho(\tau)d\tau$$

The mean lifetime for the distribution $\varrho(\tau)$ is [42]

$$< \tau >= h\tau_{kww}\Gamma[h]$$

which can be used for the FLIM map. An additional parameter h is a measure of the width of the distribution[1]. [1][4][6]

4.3.1 Application of StrEF (case 1)

The StrEF fit is tested by Siegel and co-workers [4] for its potential in differentiating between different types of biological tissue (Figures in next page) based on endogenous fluorophores such as NADH, elastin, collagen etc. It performed faster (4 vs. 5 fitting parameters) and more accurately than biexponential fit. Moreover, as the authors suggest, this approach represents the underlying biophysics in a better way.

The imaging of the parameter h, which is a measure of the width of the distribution, provides an additional contrast. The authors, considering the importance of in vivo studies, developed an experimental FLIM endoscope (Figure 4.8). As they admit though, the low SNR because of technical reasons, proved to favor the monoexponential fitting which provided better differentiation of the tissue. Nonetheless, despite the long acquisition time necessary for the endoscope now, they expressed their belief that in the future the clinical requirements for in vivo use will be reached [4].

[1] Γ[h]: Gamma Function

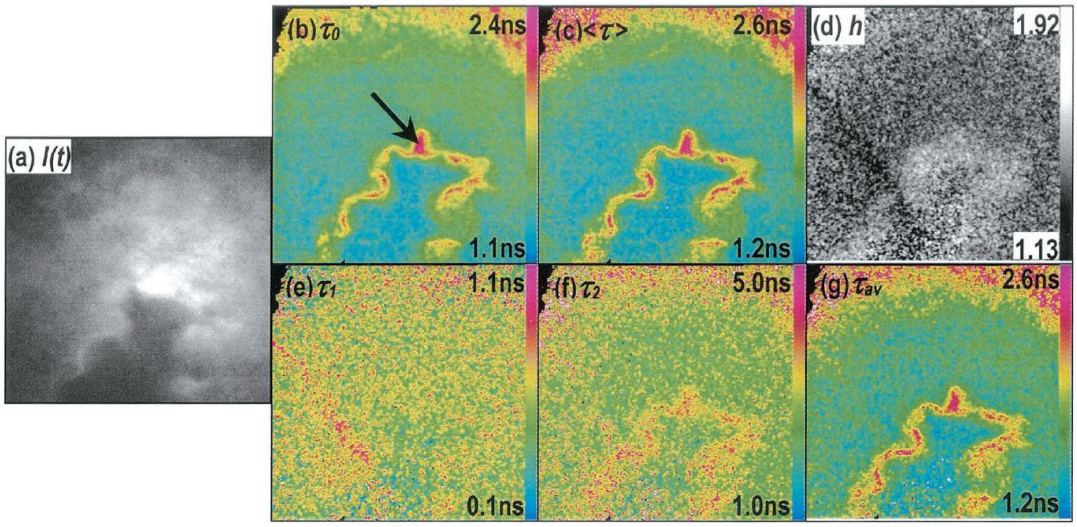

Figure 4.6. Comparison for different decay models for 15μm-thick unstained rat section X100 *

(a): Time-gated fluorescence image	(e)-(g): FLIM map for biexponential fit
(b): FLIM map from monoexponential fit: τ	(e): fast decay lifetime τ_1
(c): FLIM map from strEF fit: $<\tau>$	(f): fast decay lifetime τ_1
(d): Heterogeneity map from strEF fit: h.	(g): the physical meaningless average lifetime of τ_1,τ_2

*: the arrow in (b) shows a pixel whose decay fitting is presented below (Figure from [4])

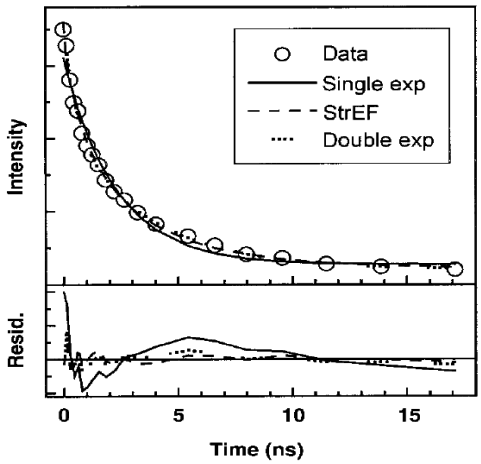

Figure 4.7. A single pixel decay from the artery wall (arrow in Figure 4.6). The lower part shows the residuals. Although the biexponential fit performs well, the assumption that there is either just one type of fluorophore with two distinct lifetimes or two distinct fluorophores with separate lifetimes in this heterogenous biological tissue is highly improbable. (Figure from [4])

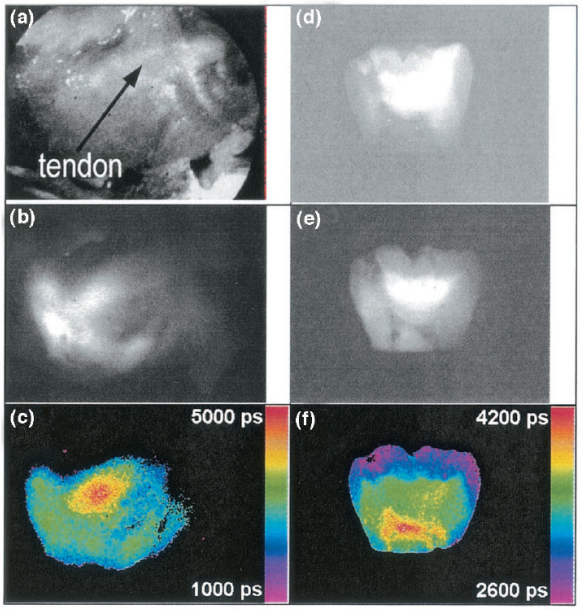

Figure 4.8.

Endoscopic images of a rabbit joint

(a): dc white light reflection

(b): time-gated fluorescence intensity

(c): FLIM map showing the different regions

Tendon-bone joint clearly contrasted

Endoscopic images of a longitudinal section of a human tooth

(d): dc white light reflection images

(e): time-gated fluorescence intensity

(c): FLIM map showing the different regions

Outer enamel, dentine and root canal are clearly contrasted

(Figure from [4])

Comment: Siegel and co-workers [4] attempted the derivation of the distribution function with an inverse Laplace transformation, which is an ill-posed problem, in the sense that a lot of combinations of contributions and lifetimes give an acceptable fit, and small errors can change dramatically the result. So, what they present is a very wide distribution for the lifetime with FWHM of 9.8ns (Figure 4.9). This difficulty leads to the need for a better approach and the method of maximum entropy, which follows, seems to be more promising [1].

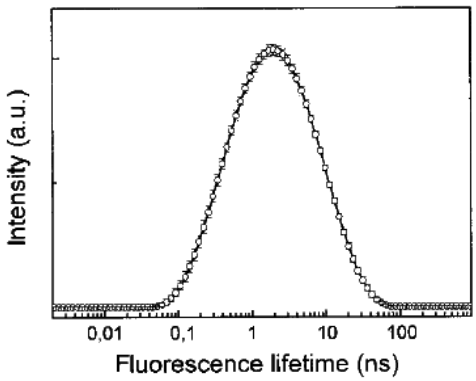

Figure 4.9. The distribution of lifetimes extracted by CONTIN (the algorithm used) from experimental decay data of a single pixel (the one shown with the arrow in Figure 4.6)

(Figure from [4])

4.3.2 Application of StrEF (case 2)

Benny and co-workers [6] use a time-gated CCD camera and a StrEF fit to differentiate between rat tissue, presenting very similar to the previous case arguments for the benefits of the StrEF approach.

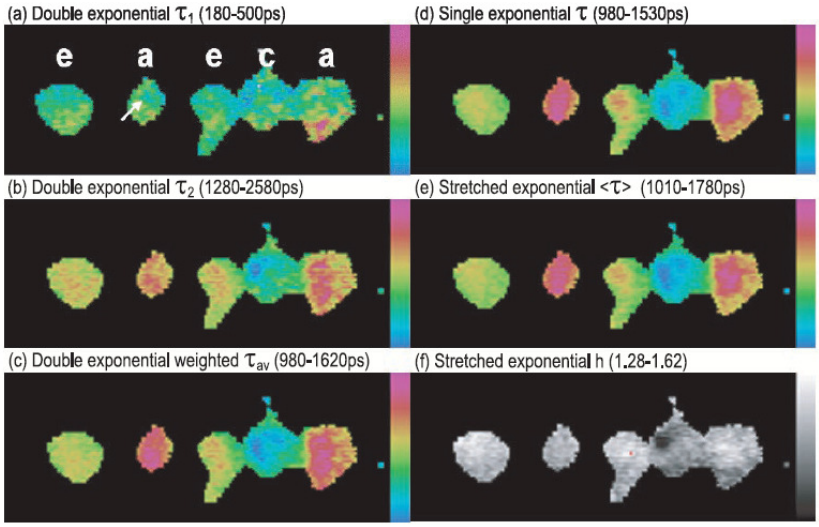

Figure 4.10. In (a) the different types of tissue are presented and their differentiation [6] e: elastin, a: aorta, c: collagen – all from rat

(a): Biexponential fit – short lifetime distribution τ_1

(b): Biexponential fit – long lifetime distribution τ_2

(c): Biexponential fit – weighted average of lifetimes

(d): Monoexponential fit – lifetime distribution τ

(e): StrEF function – mean lifetime $<\tau>$

(f): StrEF – heterogeneity parameter distribution h

(Figure from [6])

Comment: While the authors [4][6] argue against the biexponential fitting and the weighted average lifetime map, as having no physical meaning, they use the mean lifetime $<\tau>$ of the stretched function in their FLIM maps, which could also be meaningless. In the case for example where the distribution presents two peaks, the mean value is as meaningless as the weighted average for biexponential curve. However, while the StrEF mean lifetime performs better than the averaged biexponential lifetime on the tissue differentiation no specific model expalining this success is provided (Figures 4.6, 4.10).

4.4 Maximum Entropy Method (MEM)

Fluorescent molecules in heterogeneous media can be in different environments whose structure does not change in time intervals comparable to their lifetime. As it is mentioned before, in such a case the fluorophore could decay multiexponentially or it might be possible that its decay is characterized by a continuous distribution of lifetimes. Examples mentioned [16] (with references) are a pentamodal distribution in bacteriorhodopsin containing eight tryptophans, a quadrimodal distribution in horse heart apocytochrome c containing a single Trp protein etc.

The maximum entropy method (MEM) which does not make any assumptions beforehand about the lifetimes, is able to fit the decay allowing a continuous distribution $\varrho(\tau)$ of lifetimes:

$$I(t) = \int_0^\infty \exp\left(-\frac{t}{\tau}\right)\rho(\tau)d\tau$$

Among the huge set of allowable solutions (after rejecting those that contain physical contradictions) the MEM approximated distribution $\varrho(\tau)$ should minimize the chi square function:

$$\chi^2 = \frac{1}{M}\sum_{i=1}^{M}\frac{1}{\sigma_i^2}\left\{(\mathrm{I}_c(t_i) - \mathrm{I}_e(t_i)\right\}^2$$

where $I_c(t_i)$ is the calculated intensity, $I_c(t_i)$ is the experimental intensity, σ_i is the standard deviation for the i^{th} data point with M data points, and at the same time should maximize the Shannon-Jaynes entropy function defined as:

$$S = -\sum p_i \log p_i$$

where $p_i=\alpha_i/\Sigma\alpha_i$. If there is an a priori assumption for the distribution S, it takes the form:

$$S = -\sum p_i \log(p_i \,/\, m_i) \qquad [16][15][1][8]$$

4.4.1 Application of MEM (case 1)

Swaminathan and co-workers [16] after applying MEM for a sample of tryptophan in water to receive a bimodal lifetime distribution, they studied with simulated data whether the width of the lifetime distribution could serve as a quantitative measure of the heterogeneity.

Overall, it was shown that the SNR, the discretization of the lifetimes in calculations, the stopping-criterion and the completeness of the decay curve were shown to influence the width of the peaks on the lifetimes distribution, so that this cannot be a good indication for the heterogeneity of the lifetimes.

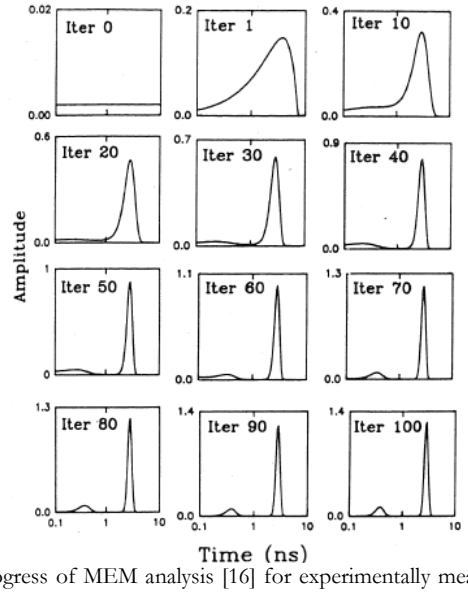

Figure 4.11. Progress of MEM analysis [16] for experimentally measured fluorescence of tryptophan in water. Starting with a flat distribution in successive iterations the distribution becomes bimodal. Initial χ^2 value is 177 (0 iterations), quickly drops to 1.66 (30 iterations) but then more gradually reaches finally 1.06 (100 iterations). The shape of the distribution for each peak is best approximated by a Gaussian function in log(τ) space. The area under each peak gives the fractional contribution of the species.
(Figure from [16])

Comment: The authors used simulated data for their study convoluting them with a realistic IRF and added the Gausian noise afterwards, which is not what really happens in an experiment. Gaussian noise is equivalent to Poisson for counts over 25, so they cut off the tail of the decay (counts<25). Having bad SNR ($\approx\sqrt{25}$) or signal with wrongly simulated noise (but positive counts) might be better than not having at all. This cut off probably shortened the run time or the data were anyway unreliable because of the discretization and the convolution. However, later they calculate the effect of the completeness of the decay on the success of MEM and it was shown that, with decays more complicated than monoexponential, a complete decay curve is crucial for the success of MEM.

4.4.2 Application of MEM (case 2)

Globular proteins, even though very efficient, fail in certain conditions to maintain or acquire their correct three dimensional structure and become dysfunctional. Amyloidosis, Parkinson's and other neurodegenerative diseases are the result of the deposition of ordered and filamentous aggregates of proteins (amyloid fibrils) on organs and tissues, inside or outside the cells. Thioflavin S and T (ThS, ThT) form amyloid-like fibrils and are very important in the study of the protein misfolding because of their spectral properties. ThT is a single molecular species (Figure 4.12). The significant change in fluorescence properties of ThT when it binds to amyloid fibrils, although not well understood, has made this molecule a very commonly used tool for the analysis of aggregating systems [26].

An equivalent parameterized (μ) criterion for the MEM is expressed [15], postulating that S should maximize ψ:

$$\psi = S - \mu(\chi^2 - 1)$$

Good choice of μ produces a smooth curve and minimizes χ^2 [15]. S in the continuous space takes the form:

$$S = \int_0^\infty \left[\alpha(\tau) - m(\tau) - \alpha(\tau) \log \frac{\alpha(\tau)}{m(\tau)} \right] d\tau$$

where m(τ) is the initial distribution (usually constant).

Stsiatura and co-workers [15] validate a MEM method they developed for deciding whether a fluorescent decay is better described by an exponential-discrete or a continuous distribution of lifetimes by studying the decay kinetics of Thioflavin T (ThT) intercalated into amyloid fibrils. From previous work ([26][43]) it was known that the torsional relaxation of the aminobenzene and benzothiazole rings, as the only nonradiative de-excitation process, determines the change in the lifetime of ThT.

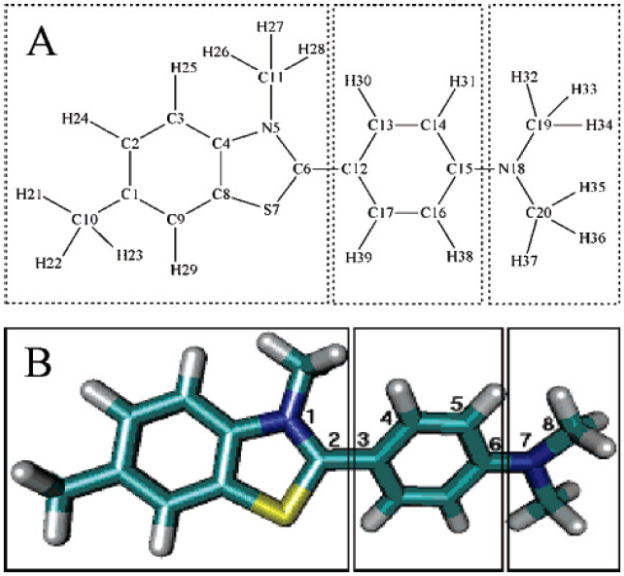

Figure 4.12. "ThT structure. (A) Chemical structure of the ThT cation. (B) Three-dimensional model of the ThT cations. S, C, and N atoms are shown in yellow, light blue, and dark blue, respectively, whereas hydrogen atoms are gray. Three ThT fragments are shown: benzthiazole ring (I), benzene ring (II), and dimethylamino group (III). Atoms forming torsion angles φ (N5-C6-C12-C13) and ψ (C14-C15-N18-C19) are numbered in B. These angles are used to characterize the potential ThT configurations in the ground and the excited states." (Figure and caption taken from [26])

The measured fluorescence decay of ThT in the amyloid fibrils needs a three-exponential fit to be approximated; while in viscous solvents it is fitted very well with a Gaussian distribution centered at the emission lifetime. This is an indication of heterogeneity when ThT is intercalated into the amyloid fibrils. After applying the MEM analysis, the distribution that was produced was a bimodal one. Although both approaches (three-exponential, bimodal distribution) give a good fit, the question is which of the two descriptions should be used to represent the mechanisms that underlie the change of the decay curve. The authors thought to adjust one parameter of the experiment and check which of the two models could be adjusted too, in order to describe successfully the decay curve, with a reasonable change in the model parameters. Thus, they added to the solution the anionic quencher KI (40mM), which significantly reduced the average lifetime. The three-exponential model gave a good fit by reducing the lifetimes of all the components and mostly the shortest. That would mean that the quencher interacted more with these molecules and consequently, one would expect the contribution of this component to decrease, which did not happen. On the other hand, the new lifetime distribution with the MEM method showed an almost parallel shift for the peaks to the lower lifetimes and the contribution for the short lifetime having drastically increased. This is in accordance with the Stern-Volmer equation for collisional quenching predicting larger decrease for the longer lifetime components [15][8].

So, the authors conclude that the MEM method can be successfully used to determine if the lifetime distribution can be described by a discrete or a continuous spectrum.

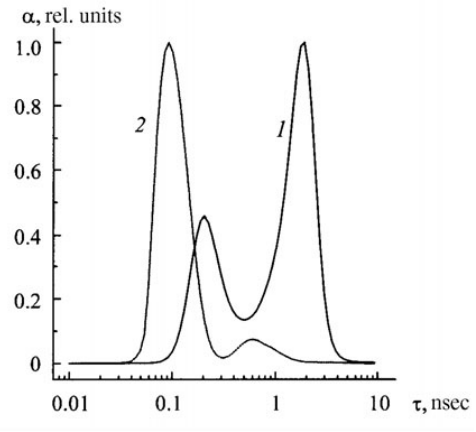

Figure 4.13. Fluorescence lifetime distribution for the ThT intercalated into amyloid fibrils.

1: Before the addition of quencher

2: After the addition of 40mM KI

(Figure from [15])

Comment: It would be interesting if the authors tried to quantify this shifting of the lifetime distribution peaks. By using a series of different concentrations of KI, they could observe and test the gradual transition from one distribution to the other for the MEM case and the possibly random change in the contributions and lifetimes for the three exponential fit case.

4.5 Implemented FLIM Medical Instruments

4.5.1 FLIM Scanning Confocal Endomicroscope

Kennedy and co-workers [5] recently presented a FLIM TC-SPC endomicroscope.

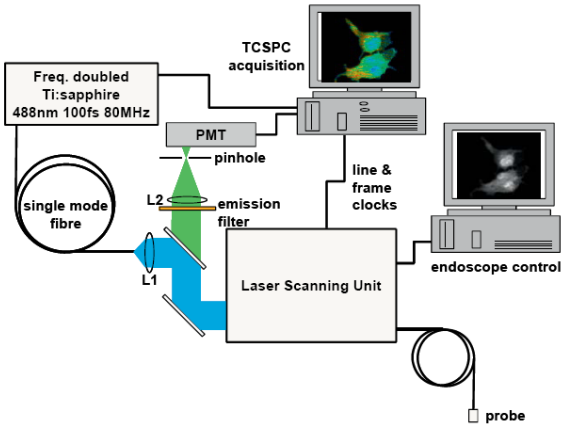

Figure 4.14. The set up of the FLIM TC-SPC endoscope attached to a licensed for clinical use endomicroscope. Kennedy and co-workers managed to reduce the acquisition time to ~1s.

(Figure from [5])

4.5.2 FLIM Endoscope for image-guided brain surgery

Sun and co-workers [44] developed a FLIM endoscope based on a gated intensified CCD camera that differentiates between normal and cancerous brain tissue during surgery based on NADH fluorescence lifetimes.

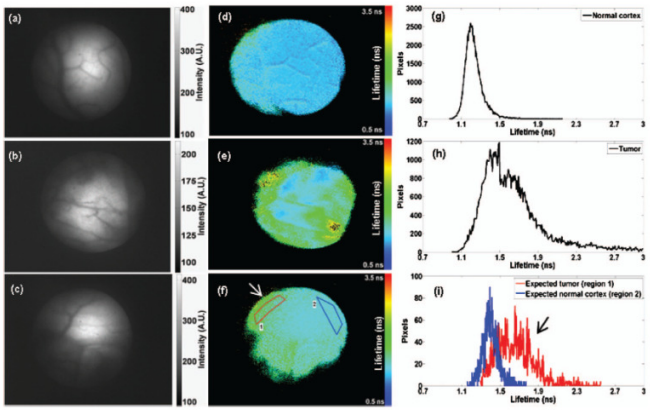

Figure 4.15
(a), (b), (c) intensity images
(d), (e), (f) average lifetime maps
(g), (h), (i) average lifetime distributions

For healthy tissue (a, d, g) a sharp lifetime distribution shows uniformity while cancerous tissue (b, e, h) exhibits wider distribution with higher average.

Tissue from brain-tumor interface (c, f, g) exhibits both distributions depending on the selected part.

(Figure from [44])

5 Conclusions - Future

FLIM imaging provides sensitivity on many parameters of the cell microenvironment combined with reliability, high temporal and spatial resolution, making use of a great variety of techniques. The recent instrumentation progress alone though, cannot be productive unless accompanied by the interdisciplinary use of principles from physics, mathematics and biology. Biomedical applications of FLIM especially, requiring short acquisition times, reliable and efficient computational methods, deeper understanding of the molecular biology of the cell and all that integrated in a light and affordable set up is an area that needs to be benefited by the interdisciplinary approach. [7][2][1]

6 Acknowledgements

I would like to thank my two supervisors, Angus Bain and Michael Duchen, as well as Thomas Blacker for their help, guidance and support during this project. My studying at UCL CoMPLEX is possible because of my scholarship by the Greek State Scholarship Foundation (IKY). CoMPLEX is an EPSRC funded Doctoral Training Centre.

7 Appendix A

Jablonski Diagram

The Jablonski diagram illustrates the transitions between the electronic states of a molecule. The horizontal lines represent the different electronic energy levels and they are grouped in S_0 (ground state) and S_1 (excited state) which are singlet states (antiparallel electron spins) while a triplet state T_1 (parallel electron spins) is also shown. In each electronic state there are a number of vibrational levels with small energy difference.

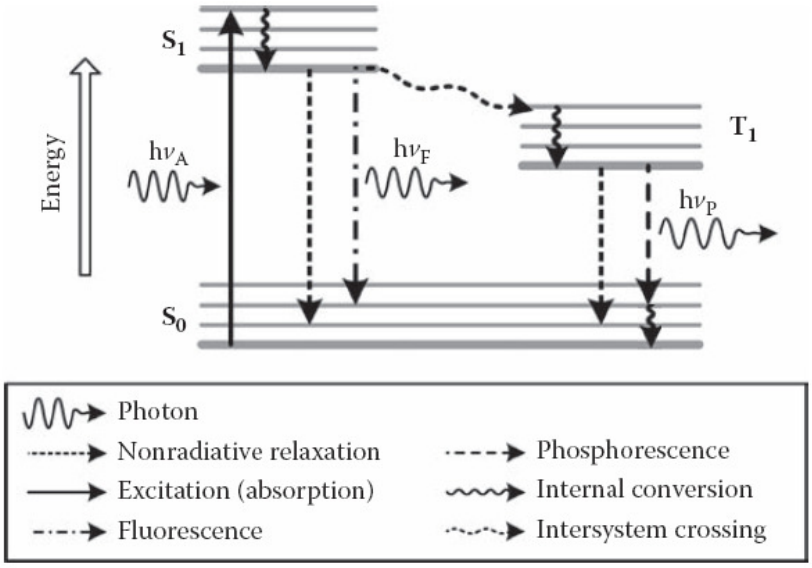

Figure A.1. Jablonski diagram

According to the Frank-Condon principle, the transitions of electrons are so rapid (vertical transitions) that no significant change in their environment occurs during this short time interval (e.g. molecular vibrations). [1][45]

(Figure from [36] with added internal conversion in S_0)

The large energy gap between ground and excited states means that at room temperature light is necessary to excite an electron. Fluorescence occurs when an excited electron from a singlet state returns to the ground state with the emission of a photon. On the other hand, phosphorescence occurs when an electron from a triplet state returns to the ground state. In the first case, the transition is allowed because of the spin pairing, so it happens rapidly resulting in a fluorescence lifetime of the order of nanoseconds. In the latter case though, it is not allowed unless spin-orbit coupling is large (when heavy atoms are present in the molecule) resulting in phosphorescence lifetimes of the order of milliseconds or even larger. The excited atom can get in a triplet state through a non-radiative transition from a singlet state, as long as there is strong spin-orbit coupling, a process which is called intersystem crossing.

Because of the overlapping among the closely located vibrational levels, molecules in a high vibrational level are quickly (10^{-12}s) relaxed to the lowest vibrational level - a process called

internal conversion, which is a sequence of radiationless transitions. Therefore absorption and emission have to do mainly with transitions from the lowest vibrational energy. Additionally, the wavelength of the exciting photon does not influence, in general, the emission spectrum.

Since nuclear geometry is not affected by the change in electronic states, the vibrational energy levels are similar in each state. This results in mirror symmetry between the corresponding absorption and emission spectra. The loss of energy however, due to vibrational de-excitation, results in a Stokes shift which means that the fluorescence emission spectrum is shifted to longer wavelengths compared to that of the absorbed photons.

The probability for a triplet molecule to deactivate is much less than that of the fluorescence deactivation. Moreover, the triplet state, because of the unpaired electron, is very reactive. Therefore, it is very probable that a molecule in a triplet state can react with other molecules, such as oxygen, which exist normally in the cell environment. Oxygen, in particular, after this interaction will become singlet, which is highly reactive and will, in turn, alter other molecules. It is almost certain that after a number of absorbed photons, the molecule will react irreversibly according to this procedure, and it will not fluoresce any more. This is called photolysis or photobleaching and it depends on the duration and intensity of illumination and the chemical environment of the fluorophore.[36][9][2][8][3][1][45]

8 Appendix B

A Global Analysis Mathematical Approach

The mathematical approach of Laptenok and co-workers [11] applying global analysis in order to estimate the distance of the donor-acceptor pair is presented:

The differential equations for the excited populations of donor D(t) and acceptor A(t) are

$$\begin{cases} \dfrac{dD(t)}{dt} = -(k_d + k_t)D(t) \\ \dfrac{dA(t)}{dt} = D(t)k_t - A(t)k_a \end{cases}$$

where $k_d=k_n+k_{nr}$ is the de-excitation rate constant for the donor, k_a is the de-excitation rate constant for the acceptor and k_t is the FRET energy transfer rate constant. The solution for the acceptor includes a negative term which expresses the rise in fluorescence. If acceptors are excited only because of the FRET then the rate of the rise of the fluorescence of the acceptor is equal to the rate of the decay of the fluorescence of the donor (for donors in Forster radius).

The processing of the data is done with global analysis. By arranging the pixels of a FLIM image in rows so as in each column the time series of the decay of a single pixel is placed, the matrix $\boldsymbol{\Psi}$ is created:

$$\boldsymbol{\Psi} = \begin{array}{c|cccc} & \chi_1 & \chi_2 & \cdots & \chi_n \\ \hline t_1 & \psi(t_1,\chi_1) & \psi(t_1,\chi_2) & \cdots & \psi(t_1,\chi_n) \\ t_2 & \psi(t_2,\chi_1) & \psi(t_2,\chi_2) & \cdots & \psi(t_2,\chi_3) \\ \vdots & \vdots & \vdots & & \vdots \\ t_m & \psi(t_m,\chi_1) & \psi(t_m,\chi_2) & \cdots & \psi(t_m,\chi_n) \end{array}$$

$\psi(t_i,\chi_i)$ is the fluorescence intensity at time t_i in pixel χ_i.

The multiexponential decay is convolved with the instrument response function p(t) to give the total fluorescence for a pixel.

$$F(t) = \sum_{q=1}^{Q} \alpha_q \exp(-\frac{t}{\tau_q}) \otimes p(t)$$

The IRF can be measured but is not analytically known so an iterative reconvolution [47] must be performed for each decay component. Applying the global analysis constrain that for each pixel the lifetimes of the components are identical, the matrix $\boldsymbol{\Psi}$ takes the form:

$$\mathbf{\Psi} = \mathbf{C}\,\mathbf{A}^T + \mathbf{Z} \;=\; \sum_{q=1}^{n_{comp}} c_q\,\alpha_q^T \;+ \mathbf{Z} \;=\; \sum_{q=1}^{n_{comp}} \left(\exp(-\frac{t}{\tau_q}) \otimes p(t) \right) \alpha_q^T \;+ \mathbf{Z}$$

The product of **C**, $\mathbf{A}^T$ represents the dataset for one FLIM image and **Z** is an additive Gaussian noise. A column in matrix **C** represents the time series of decay for one component while a row of $\mathbf{A}^T$ represents the contribution of the component for each pixel. The noise follows Poisson distribution and it is approximated by Gaussian as long as the number of photon counts is large (ref. [46] in [11]). The estimation of the Q lifetimes and the n elements (one for each pixel) of the Q (for every component) α vectors is a separable non-linear least squares optimization problem and can be confronted with already developed algorithms [38][2].

9 Appendix C

Multiple Frequency Fluorescence Lifetime Imaging Microscopy

A frequency-domain FLIM technique, called multiple-frequency Fluorescence Lifetime Imaging Microscopy (mfFLIM), which can resolve complex decays and does not require frequency scanning, is described by Squire and co-workers [20]. In mfFLIM the sample is excited by light which is modulated by a sum of harmonics using standing wave acousto-optic modulators (AOMs) in series and the emission fluorescence is analyzed by homodyne detection at each harmonic frequency simultaneously.

The fluorescence response R(t) for Q species with lifetime τ_q after a δ-excitation, is the sum of all the exponential decays.

$$R(t) = \sum_{q=1}^{Q} \frac{\alpha_q}{\tau_q} \exp\left(\frac{-t}{\tau_q}\right) \tag{C.1}$$

where α_q are the fractional contributions to the steady-state fluorescence of the different species. The relative populations a_q are related to the fractional contributions α_q, if the species have common spectrum, by a multiplication with the lifetimes and a renormalization constant [1].

The intensity of the excitation light is not a single sinusoidal signal but a set of harmonics; thus, it can be written as a Fourier series, with ω being the fundamental frequency, N the number of the significant harmonics, E_0 the mean intensity, E_n the amplitude of the n^{th} harmonic and $\phi_{E,n}$ its phase [37]:

$$E(t) = E_0 + \sum_{n=1}^{N} E_n \cos(n\omega t + \phi_{E,n}) \tag{C.2}$$

It is convolved with the response function R(t) of the sample to give the fluorescence of the sample as a function of time:

$$F(t) = E_0 + \sum_{n=1}^{N} E_n M_n \cos(n\omega t + \phi_{E,n} - \Delta\phi_n) \tag{C.3}$$

The phase shift of each harmonic $\Delta\phi_n$ and its modulation M_n are related to the fractional contributions α_q and lifetimes τ_q with the equations:

$$\Delta\phi_n = \arctan\left(\frac{A_n}{B_n}\right) \tag{C.4.a}$$

$$M_n = \sqrt{A_n^2 + B_n^2} \tag{C.4.b}$$

where,

$$A_n = \sum_{q=1}^{Q} \frac{\alpha_q n\omega\tau_q}{1 + (n\omega\tau_q)^2} \tag{C.5.a}$$

$$B_n = \sum_{q=1}^{Q} \frac{\alpha_q}{1 + (n\omega\tau_q)^2} \tag{C.5.b}$$

So, one can determine the α_q and τ_q for each species from equations (C.5), using a non-linear fit to minimize the χ^2 function after having measured the $\Delta\phi_n$ and M_n for each harmonic.

$$\chi^2 = \sum_{n=1}^{N} \frac{1}{\sigma^2_{\Delta\phi_n}} (\Delta\phi_n - \Delta\phi_{cn})^2 + \sum_{n=1}^{N} \frac{1}{\sigma^2_{M_n}} (M_n - M_{cn})^2 \tag{C.6}$$

where $\Delta\phi_{cn}, M_{cn}$ are the calculated phase shifts and modulations respectively while the $\sigma^2_{\Delta\phi_n}$ and $\sigma^2_{M_n}$ are the estimated uncertainties for the measured quantities.

The determination of the $\Delta\phi_n$ and M_n however, is not direct. It requires first, multiplication of the F(t) with another high frequency signal G(t) of the same (homodyne) fundamental ω frequency through a high-speed image intensifier device (Microchannel Plate or MCP). The modulation of the cathode voltage of the MCP by a sinusoidal signal of frequency ω creates a square-pulse modulation for the emission, with harmonics whose amplitude (and number) can be varied by adjusting the off-set of the sinusoidal signal. The frequency mixing gives a signal of a time-independent component together with a multitude of oscillations at the harmonic frequencies and frequencies which are the sum or the difference of the frequencies of the harmonics (Figure C.1)[37].

All the time-dependant components can be filtered out, with a low pass filter (slow response of the photoluminescence surface), allowing only the independent of the time signal D(k) to pass:

$$D(k) = QE\left(G_0 F_0 + \frac{1}{2}\sum_{n=1}^{N} F_n G_n \cos(\phi_n - nk\Delta\varphi) \right) \qquad \text{(C.7)}$$

where QE expresses the photon detection efficiency and the fluorophore quantum yield, G_0 is the average G(t) signal, G_n is the amplitude of each harmonic of the G(t), ϕ_n the phase difference for each harmonic between fluorescence and G(t) and $k\Delta\varphi$ is a phase difference which can be adjusted by changing the phase of G(t). D(k) can be sampled for various phases of the G(t) (k=1, 2, … for same intervals), giving a sequence of phase dependent images. Sampling[1] of the D(k) over a period of the fundamental harmonic, allows the Fourier decomposition for every frequency and subsequently, the estimation of the phase shifts ϕ_n and the amplitudes $\frac{1}{2} G_n F_n$ for each harmonic. These are simply related to the $\Delta\phi_n$ and M_n which can be calculated afterwards.

In the simple case of monoexponential decay, equations (C.4), (C.5) can be solved easily to give the lifetime:

$$\tau_{\Delta\phi,n} = \frac{\tan(\Delta\phi_n)}{n\omega} \qquad \text{(C.8.a)}$$

$$\tau_{M,n} = \frac{\sqrt{\frac{1}{M_n^2} - 1}}{n\omega} \qquad \text{(C.8.b)}$$

They should give both, the same result for the lifetime, independently of the frequency. Therefore, at the same time, they provide an indication of whether the decay is indeed monoexponential. [17][36][20] [37][46][47][48]

[1] The number of samples is determined by the Nyquist criterion i.e. sampling rate of at least twice of the highest harmonic, $f_S \geq 2f_N$

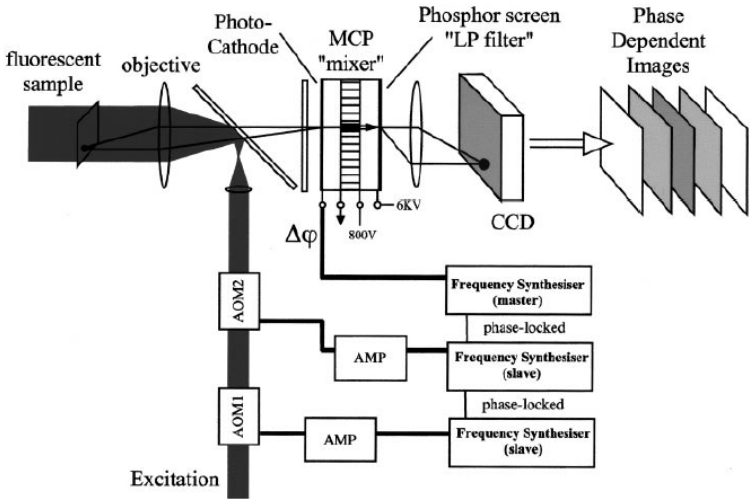

Figure C.1. Schematic diagram of mfFLIM. A frequency synthesizer (master) modulates the photocathode voltage of the MCP and is also phase-locked with two other frequency synthesizers (slaves) that drive the two AOMs (acousto-optic modulators) placed in series modulating the excitation light at four harmonics. The mixing of the fluorescent light with the square pulse is done at the MCP and the intensity is recorded by a CCD camera. By varying the phase of the master synthesizer, a series of phase dependent images is created. From the Fourier decomposition of the intensity data for each pixel, the phase shifts and the relative modulations are determined. (Figure from [37])

10 References

1. Valeur B 2002 *Molecular Fluorescence* (Wiley-VCH)
2. Borst J W and Visser A J W G 2010 Fluorescence lifetime imaging microscopy in life sciences *Meas. Sci. Technol.* **21** 102002
3. Festy F, Ameer-Beg S M, Ng T and Suhling K 2007 Imaging proteins in vivo using fluorescence lifetime microscopy *Mol. BioSyst.* **3** 381-391
4. Siegel J, Elson D S, Webb S E D, Lee B K C, Vlandas A, Gambaruto G L, Leveque-Fort S, Lever M J, Tadrous P J, Stamp G W H, Wallace A L, Sandison A, Watson T F, Alvarez F and French P M W 2003 Studying biological tissue with fluorescence lifetime imaging: microscopy, endoscopy, and complex decay profiles *Appl Opt.* Jun 1; **42**(16):2995-3004.
5. Kennedy G T, Manning H B, Elson D S, Neil M A A, Stamp G W, Viellorobe B, Lacombe F, Dunsby C and French P M W 2010 A fluorescence lifetime imaging scanning confocal endomicroscope *J. Biophoton.* **3** No. 1-2 103-107
6. Lee B K C, Siegel J, Webb S E D, Leveque-Fort S, Cole M J, Jones R, Dowling K, Lever M J and French P M W 2001 Application of the Stretched Exponential Function to Fluorescence Lifetime Imaging *Biophysical Journal,* **81**, Issue 3, 1265-1274
7. Suhling K, French P M and Wand Phillips D 2005 Time-resolved fluorescence microscopy *Photochem. Photobiol. Sci.* **4** 13–22
8. Lakowicz J R 2006 *Principles of Fluorescence Spectroscopy* Third Edition (New York: Springer)
9. Berland K 2001 *Basics of Fluorescence, Methods in Cellular Imaging* (ed. A. Periasamy) Oxford University Press pp. 5-19
10. Wang X F and Herman B (ed) 1996 *Fluorescence Imaging Spectroscopy and Microscopy* (New York: John Wiley & Sons)
11. Laptenok S P, Borst J W, Mullen K M, van Stokkum I H, Visser A J and van Amerongen H 2010 Global analysis of Förster resonance energy transfer in live cells measured by fluorescence lifetime imaging microscopy exploiting the rise time of acceptor fluorescence *Phys Chem* **12**, 7593-602.
12. Mielczarek E V, Greenbaum E, Knox R S (eds) 1993 *Biological Physics American Institute of Physics* p.148 (a translation from the German: Forster T 1948 Intermolecular energy migration and fluorescence *Annalen der Physik* ser. 6 vol. **2**
13. Vliet P C and Pillai S (ed) 2009 Laboratory Techniques in Biochemistry and Molecular Biology 33 (Amsterdam: Elsevier)
14. Becker W 2005 *Advanced Time-Correlated Single Photon Counting Techniques* (Berlin: Springer)
15. Maskevich A A, Stsiapura V I and Balinski P T 2010 Analysis of fluorecence decay kinetics of Thioflavin T by a maximum entropy method Journal of *Applied Spectroscopy* **77** No. 2
16. Swaminathan R, Periasamy N 1996 Analysis of fluorescence decay by the maximum entropy method: Influence of noise and analysis parameters on the width of the distribution of lifetimes *Chem. Sci.* **108** No. 1
17. Verveer P J, Squire A and Bastiaens P I 2000 Global analysis of fluorescence lifetime imaging microscopy data *Biophys J* **78**, 2127-37
18. Application Note 2008 *Recording the Instrument Response Function of a Multiphoton FLIM* Becker & Hickl GmbH

19. Gratton E, Limkeman M, Lakowicz J R, Maliwal B P, Cherek H and Laczko G 1984 Resolution of mixtures of fluorophores using variable-frequency phase and modulation data *Biophys J* **46**, 479-86.

20. Squire A and Bastiaens P I 1999 Three dimensional image restoration in fluorescence lifetime imaging microscopy *J Microsc* **193**, 36-49

21. Lakowicz J R, Laczko G, Cherek H, Gratton E and Limkeman M 1984 Analysis of fluorescence decay kinetics from variable-frequency phase shift and modulation data *Biophys J* **46**, 463-77

22. Lakowicz J R, Szmacinski H, Nowaczyk K and Johnson M L 1992 Fluorescence lifetime imaging of free and protein-bound NADH *Proc. Natl. Acad. Sci. USA***89** 1271–1275.

23. Verveer P J and Bastiaens P I 2003 Evaluation of global analysis algorithms for single frequency fluorescence lifetime imaging microscopy data *J Microsc* **209**, 1-7

24. Bastiaens P I and Squire A 1999 Fluorescence lifetime imaging microscopy: spatial resolution of biochemical processes in the cell *Trends Cell Biol.* **9** 48–52

25. Livesey A K and Brochon J C 1987 Analyzing the distribution of decay constants in pulse-fluorimetry using the maximum entropy method *Biophysical Journal* **52** 5 693-706

26. Maskevich A A, Stsiapura V I, Kuzmitsky V A, Kuznetsova I M, Povarova O I, Uversky V N and Turoverov K K 2007 Spectral Properties of Thioflavin T in Solvents with Different Dielectric Properties and in a Fibril-Incorporated Form *J. Proteom Res.* **6** (4) 1392-1401

27. Masters T A, Calleja V, Armoogum D A, Marsh R J, Applebee C J, Laguerre M, Bain A J, Larijani Banasfshe 2010 Regulation of 3-phosphoinositide–dependent protein Kinase 1 activity by homodimerization in live cells *Sci. Signal.* **3** 145

28. Perrin F 1929 La fluorescence des solutions *Ann. Phys.* Paris **12** 169-275

29. Bird D K, Yan L, Vrotsos K M, Elicieri WK, Vaughan E M, Keely P J, White J G and Ramanujam N 2005 Metabolic mapping of MCF10A Human Breast Cells via multiphoton fluorescence lifetime imaging of the coenzyme NADH C*ancer Res* **65** (19)

30. Skala C M, Riching K M, Bird D K, Gendron-Fitzpatrick A, Eickhoff J, Eliceiri K W, Keely P J and Ramanujam N 2007 In vivo multiphoton fluorescence lifetime imaging of protein-bound and free nicotinamide adenine dinucleotide in normal and precancerous epithelia *J.of BioMed. Opt.* **12** 2

31. Heiden M G V, Cantley L C and Thompson C B 2009 Understanding the Warburg effect: The metabolic requirements of cell proliferation *Science* **324** 1029

32. Knutson J R, Beechem J M and Brand L 1983 Simultaneous analysis of multiple fluorescence decay curves: a global approach *Chem. Phys. Lett.* **102**:501–507

33. Beechem J M, Ameloot M and Brand L 1985 Global and target analysis of complex decay phenomena *Anal. Instrum.* **14**:379–402

34. Beechem J M, and Brand L 1986 Global analysis of fluorescence decay: applications to some unusual experimental and theoretical studies *Photochem. Photobiol.* **44**:323–329

35. Smirnov A V, Combs C A, Balaban R S, Tang K and Knutson J R 2009 A hybrid global fitting algorithm for decay-associated images from fluorescence lifetime image microscopy data *Proc. of SPIE* **7184** D-1

36. Periasamy A and Clegg R M (ed) 2009 *FLIM Microscopy in Biology and Medicine*(Chapman & Hall/CRC)

37. Squire A, Verveer P J and Bastiaens P I 2000 Multiple frequency fluorescence lifetime imaging microscopy *J Microsc* **197**, 136-49

38. Golub, G H, and Pereyra V 1973 The differentiation of pseudo-inverses and nonlinear least squares problems whose variables separate *SIAM J.Numer. Anal.* **10**:413– 432
39. Verveer P J, Squire A and Bastiaens P I 2001 Improved spatial discrimination of protein reaction states in cells by global analysis and deconvolution of fluorescence lifetime imaging microscopy data *J Microsc* **202**, 451-6.
40. Alcala J R 1994 The effect of harmonic conformational trajectories on protein fluorescence and lifetime distributions *J. Chem. Phys.* **101**:4578–4584.
41. Alcala J R, Gratton E, and Prendergast F G 1987 Fluorescence lifetime distributions in proteins *Biophys. J.* **51**:597– 604
42. Alvarez F, Alegrıa A, and Colmenero J 1991 Relationship between the time-domain Kohlrausch–Williams–Watts and frequency-domain Havriliak–Negami relaxation functions *Phys. Rev. B* **44**, 7306–7312
43. Stsiapura V I, Maskevich A A, Kuzmitsky V A, Turoverov K K and Kuznetsova I M 2007 Computational Study of Thiflavin T Torsional relaxation in the Excited State *J. Phys. Chem. A* **111** (22) 4829-4835
44. Sun Y, Hatami N, Yee M, Phipps J, Elson D S, Gorin F, Schrot R and Marcu L 2010 Fluorescence lifetime imaging microscopy for brain tumor image-guided surgery *J. Biomed. Opt* **15** 5
45. Atkins P W and Friedman R S 2005 *Molecular Quantum Mechanics* Oxford University Press
46. Golub G and Pereyra V 2003 Seperable nonlinear squares: the variable projection method and its applications *Inverse Problem* **19**, R1–R26
47. Laptenok S P, Mullen K M, Borst J W, van Stokkum I H M, Apanasovich V V and Visser A J W G 2007 Fluorescence Lifetime Imaging Microscopy (FLIM) data analysis with TIMP *J. Statist. Software* **18** 1–20
48. Clegg R M and Schneider P C 1996 *Fluorescence lifetime-resolved imaging microscopy: a general description of lifetime-resolved imaging measurements. Fluorescence Microscopy and Fluorescence Probes* (ed. by J. Slavik), pp. 15–33 (New York: Plenum Press)